CONFERENCE PRE-PRINT

HL-3 RESEARCH TOWARDS HIGH-PERFORMANCE PLASMA AND POWER EXHAUST SOLUTION

W. L. Zhong*[1], X. Q. Ji[1], W. Chen[1], X. Y. Bai[1], A. Bécoulet[2], J. Bucalossi[3], Z. Chen[1], Z. P. Chen[4], Y. H. Chen[1], N. Conway[5], L. Delpech[3], P. Diamond[6], A. Ekedahl[3], J. Garcia[3], Y. Gribov[2], W. X. Guo[4], Z. B. Guo[7], G. Z. Hao[1], J. Harrison[5], M. Huang[1], P. Huynh[3], M. Isobe[8], K. Imadera[9], M. Jiang[1], Y. Kamada[2], S. H. Kim[2], D. King[5], Y. Kishimoto[9], X. L. Liu[1], B. Li[1], J. X. Li[1], A. Loarte[2], F. Militello[5], S. Morita[8], K. Nagasaki[9], L. Nie[1], K. Ogawa[8], M. Schneider[2], Z. B. Shi[1], F. Rimini[5], H. J. Sun[5], Y. Q. Wang[1], X. G. Wang[10], H. L. Wei[1], G. L. Xiao[1], L. Xue[1], X. Xu[4], Z. Y. Yang[1], P. X. Yu[1], Y. Yu[11], B. D. Yuan[1], F. Zhang[1], J. Z. Zhang[1], Y. Zhang[1], Y. P. Zhang[1], X. Zheng[1], X. L. Zou[3], M. Xu[1], X. R. Duan[1], Y. Liu[1], L. B. Zhang[1], Ye Liu[1] and HL-3 team

[1] *Southwestern Institute of Physics, PO Box 432, Chengdu 610041, China*

[2] *ITER Organization,13067 Saint Paul Lez Durance Cedex, France*

[3] *CEA, IRFM, F-13108 Saint Paul Lez Durance, France*

[4] *Huazhong University of Science and Technology, Wuhan, China*

[5] *UKAEA, Culham Campus, Abingdon, Oxfordshire OX14 3DB, UK*

[6] *University of California San Diego, La Jolla, California 92093, United States of America*

[7] *Peking University, Beijing, China*

[8] *National Institute for Fusion Science, Oroshi, Toki, Gifu 509-5292, Japan*

[9] *Kyoto University, Uji, Kyoto, 611-0011, Japan*

[10] *Harbin Institute of Technology, Harbin 150006, China*

[11] *Sun Yat-sen University, Zhuhai 519082, China*

*Email: zhongwl@swip.ac.cn

Abstract

The HL-3 tokamak program addresses critical challenges in developing integrated high-performance scenarios compatible with power exhaust demands for ITER and future reactors. Through systematic facility enhancements including auxiliary heating upgrades to 19.5 MW and AI-enabled control systems achieving 95.5% disruption avoidance, HL-3 finished a new round of exploration and validation for high-performance operation and power exhaust solution. Result of high-performance scenarios exploration at mega-ampere plasma current includes core ion temperatures of more than 10 keV, triple products of $6.7\times10^{19}m^{-3}\cdot s\cdot keV$, and high beta scenarios with double transport barriers. Complementary edge solutions accomplish small/no ELM regimes, such as EDA and QH-mode, and a new type staircase H-mode featuring step-like ion temperature radial profiles. Physic experiments on the integration of power exhaust emphasizes on advanced divertor configurations such as snowflake and tripod that significantly decreases peak heat flux, ELM control via resonant magnetic perturbations (RMPs), the impurity mixture SMBI and LHCD and a real-time detachment feedback control. These developments establish fundamental physics and technical foundations for demonstration and extrapolation of high-performance plasma operation for ITER and future devices.

1. INTRODUCTION

The mission of the HL-3 tokamak is to advance the physics basis for high-performance tokamak operation and to develop integrated solutions for the power exhaust challenge in support of ITER and future fusion reactors. The HL-3 tokamak (I_p = 3 MA, B_T = 3 T, R = 1.78 m, a = 0.65 m, $\kappa \leq 1.8$, $\delta \leq 0.5$) with flexible magnetic configuration[1] provides a unique platform to investigate key physics and engineering challenges of high parameter plasma operation. The recent experimental campaign targeting high-performance operations has been carried out via systematic upgrades of key facilities and scenarios development by considering the optimized performance in cores with compatible solutions on the boundaries. Advances in each of these areas are summarized below. Section 2 outlines upgrades to facilities such as plasma heating systems, plasma control systems and algorithms and diagnostics. Section 3 reports experimental results on the investigations of high-performance plasma scenarios. Section 4 covers exhaust power mitigation by using advanced divertor configurations, and active actuators to manage edge heat flux and edge localized mode (ELM) instabilities and real-time feedback control system for divertor detachment. In section 5, conclusions and the future outlook are presented.

2. ENHANCEMENT OF OPERATIONAL CAPACITY

Since 2023, a range of sub-systems has been upgraded to enhance the operational capacity for the exploration of advanced plasma scenarios with high performance and power exhaust solutions. These improvements include auxiliary heating and current drive, plasma control systems and advanced algorithm and improved diagnostic systems. Collectively, they are major facilitators of scenario development and physics investigation within this experimental campaign to form a basic platform of future high-performance operation.

2.1 Auxiliary heating and current drive systems

A total heating capacity of over 40 MW, including 20 MW of neutral beam injection (NBI) with three beamlines (6 MW, 7 MW, 7 MW), 13 MW of electron cyclotron resonance heating (ECRH) (6 MW at 140 GHz or 175 GHz, 2 MW at 140 GHz, 5 MW at 105 GHz), 6 MW of ion cyclotron resonance frequency (ICRF) (4×1.5 MW at 25-50 MHz), and 4 MW of lower hybrid current drive (LHCD) (2 MW with 6×32 FAM and 2 MW with 4×32 FAM antenna) will be installed in HL-3. A combined heating capacity of 19.5 MW, comprising 12 MW NBI systems, 5.5 MW ECRH systems, and 2 MW LHCD system has been demonstrated so far in this experimental campaign. Notably, the newly installed second NBI beamline, completed in November 2024, features four ion sources (2×2 configuration) with optimized molybdenum electrodes and a focused beam design, achieving 40 A of ion current and contributing up to 3 MW injection power. As shown in Fig. 1, the commissioning data, denoted by blue dots, agree closely with the theoretical optimal perveance I-V curve of the ion source, particularly at higher voltages. Along with the first beamline, the NBI system has delivered a maximum of about 5 MW in the latest experimental campaign, providing strong support for high-performance plasma operation. The ECRH system was enhanced with newly developed high-frequency gyrotrons and flexible antenna control, significantly increasing the central electron temperature and enabling real-time NTM control. The LHCD system upgraded with new high-mode transmission components coupled 1MW power to the plasma and has achieved fully non-inductive current drive with high coupling efficiency.

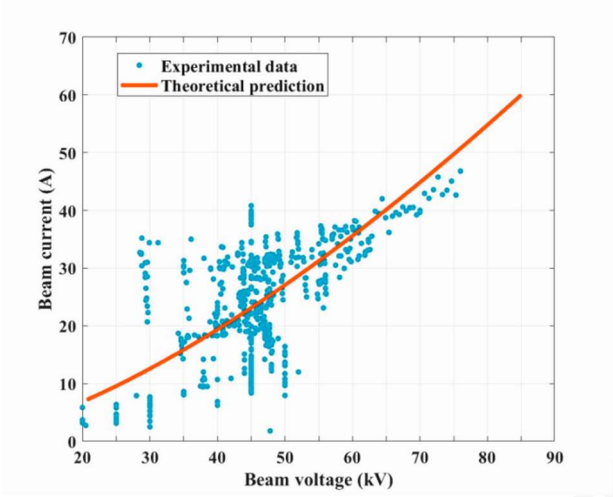

FIG.1. The beam voltage and beam current of a new ion source achieved during the last experimental campaign.

2.2 Plasma control

To complement the hardware developments, significant process has been achieved in plasma control, to achieve improved stability and real-time adaptability in the high-performance regimes. During the 2024–2025 campaign, vertical instability control system was commissioned on HL-3, consisting of an out-vessel poloidal field coil (PF2) and fast-response power supply (±1 kV/±4 kA/5 kHz) [2]. This system allowed fine control of vertical position of highly shaped plasmas ($\kappa = 1.8$, $\delta = 0.6$) using coordinated fast and slow control loops. Moreover, better real-time detection and mitigation of abnormal operational events made the plasma operations more robust, allowing discharges exceeding 1.5 MA with flat-top duration of up to four times the energy confinement time. Also, methods are implemented in the plasma control[3]. a machine learning-based predictor of disruptions, called parametric preemptive neural network (PPNN), was developed and successfully employed in closed-loop control, addressing the issue of extrapolation inherent in past models. To further improve plasma control abilities, an RL controller based on AI was implemented to manage autonomous plasma control events, enabling smooth transitions between manual and algorithmic control. The newly developed CODIS control system, which integrates operational logic, data management, and intelligent decision-making, was validated in a series of experiments. These tools, together with GPU-accelerated reconstruction in equilibrium, reach sub-millisecond timescales, and thereby build a wide-ranging real-time controlling infrastructure that is essential for reliable access to advanced operational regimes.

2.3 Plasma diagnostics

Advances in diagnostics have played a pivotal role in supporting scenario development by providing detailed, high-resolution measurements of core and edge plasma parameters. Over 40 diagnostic systems were operated during the 2024–2025 campaign[1]. Key developments include an expanded Thomson scattering system with 60 spatial channels, significantly enhancing the accuracy of electron temperature and density profiles. A multi-grating spectrometer enabled simultaneous measurements of multiple ion species, and a novel impurity calibration technique reduced measurement uncertainties by 60%, offering a benchmark methodology for ITER diagnostics. To characterize edge turbulence and mode structures, a

Doppler backscattering and cross-polarization scattering (DBS/CPS) system employing comb-frequency technology was deployed[4]. This enabled simultaneous measurement of density and magnetic fluctuations and provided the first clear observation of edge instabilities during H-mode operation. Further diagnostic advances include a far-infrared polarimeter-interferometer for current density profile reconstruction and the first successful application of two-photon absorption laser-induced fluorescence (TALIF) for measuring neutral deuterium dynamics. Together, these diagnostics provide essential support for the validation of integrated scenarios and the refinement of transport and stability models.

3. SCENARIO DEVELOPMENT TOWARDS TO HIGH-PERFORMANCE PLASMA

To support the upcoming DT campaign, HL-3 has focused on developing high-performance scenarios that achieve high core and edge pressure with scenarios such as hot ion mode, double transport barrier and super H-mode[5]. Operation scenarios characterized by high normalized beta, and small or completely ELM-free pedestal are also primary research objectives. This section summarizes recent experimental progress in establishing such scenarios.

3.1 Approaches to high temperature plasmas

Achieving high triple products and ion temperatures over 10 keV is essential to produce considerable fusion energy. The strategy on HL-3 is to achieved an internal transport barrier to increase the core ion temperature before accessing an edge transition into H-mode pedestal structure. In L-mode discharges, ion heating was enhanced by staggered NBI injection while avoiding H-mode onset through the unfavourable magnetic drift configuration, maintaining low density and facilitating efficient heating.

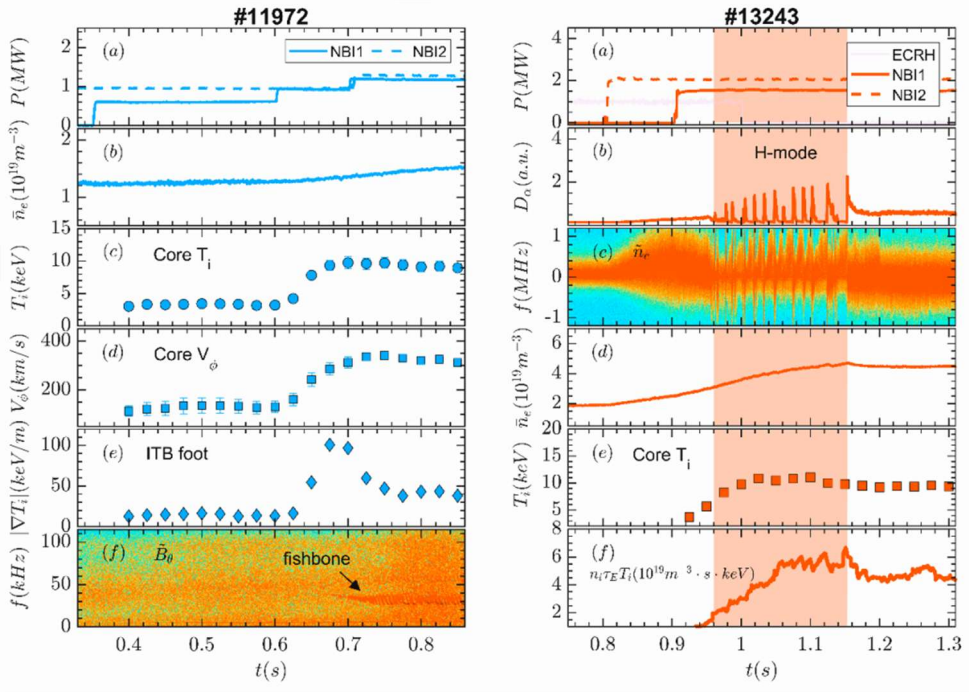

FIG.2. Left column: (a) NBI heating power of L-mode discharge #11972, (b) central-line averaged electron density, (c) core ion temperature, (d) core toroidal rotation, (e) ion temperature gradient, (f) magnetic fluctuation spectrum. Right column: (a) NBI and ECRH heating power of H-mode discharge #13243, (b) D_α emission, (c) edge density fluctuation spectrum, (d) central line-averaged electron density, (e) core ion temperature, and (f) triple product.

Left column in Fig. 2 illustrates the typical discharge (#11972) that achieved high core ion temperature. In this experiment, ion heating was provided by two neutral beam injection (NBI) systems, whose operation was deliberately time-staggered to enable stepwise power increments. The density at approximately $1.2\times10^{19}m^{-3}$ in Fig. 2(b) and unfavorable magnetic drift configuration leading to a continuously increasing of ion temperature. While further obvious increase of T_i (Fig. 2(c)) is accompanied by the increase of ion temperature gradient (Fig. 2(e)), suggesting the formation of ion internal transport barrier (ITB). It has been shown in the magnetic fluctuation spectrum that the fishbone mode appears with the ITB, indicating that the energetic particles are actively driving the instability. The observation suggests that energetic particle confinement and transport are crucial for the formation of ITB. In this scenario, the plasma density is low and the ion temperature significantly exceeds the electron temperature ($T_i/T_e \sim 3$) in the core plasma, which is the key feature of hot ion mode.

To further increase the plasma density, comparable performance was achieved in the H-mode discharges with maximum plasma current higher than 1.5MA. Right column in Fig. 2 shows a typical discharge (#13243) using sequential NBI and early ECRH application to increase ion temperature and suppressed sawteeth, stabilized the core plasma, and finally led to a sharp increase in stored energy and globe confinement during the H-mode phase. The resulting triple product reached $6.7\times10^{19}\,m^{-3}\cdot s\cdot keV$, in which the ion density is calculated by the effective Z data, and the energy confinement time was validated by thermal energy calculation from the equilibrium reconstruction. This high-performance scenarios are critical for the study of the core and edge physics and power exhaust control methods.

3.2 High β_N plasma and underlying instabilities

The high β_N scenario ($\beta_N > 3$) has been reproducibly accessed by tailoring both the current and pressure profiles as shown in Fig. 3. Reversed magnetic shear is established through early NBI heating that drives a non-inductive current, as corroborated by reversed-shear Alfvén eigenmodes. Localized ECRH is subsequently employed to suppress magnetohydrodynamic instabilities—particularly neoclassical tearing modes (NTMs)—thereby further improving the performance. Long-duration discharges with $\beta_N > 2.5$ sustained over ~15 energy confinement times were realized in plasmas with weak or reversed central shear ($q_0>1$, $q_{95}\sim4.5$). Double transport barriers (DTBs) were also achieved in low-current hybrid H-mode plasmas, enabling $\beta_N > 4$. However, NTMs were frequently observed and found to degrade confinement, sometimes leading to disruption. Core 2/1 and 3/2 NTMs have been identified as primary β_N limiters: NTMs decelerate β_N growth leading to saturation or disruptions. Meanwhile, the beta-induced Alfvén eigenmodes (BAEs) can also be excited with increasing NBI power which may degrade the confinement [6]. However, the interaction between micro-tearing mode and energetic-electron-driven geodesic acoustic mode has been found to reduce ambient turbulence, thereby improving energy and particle confinement[7].

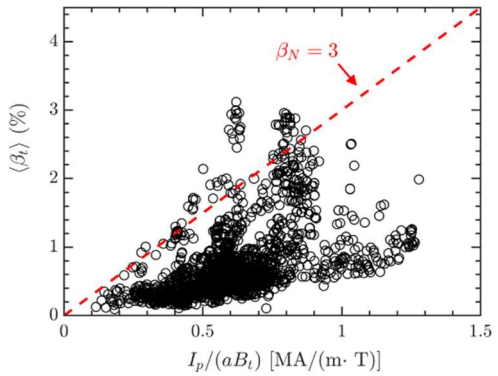

FIG. 3. Statistic results of $<\beta_t>$ versus I_p/aB_t from the recent HL-3 discharges. The red circles represent the shots with β_N over 3.

The experimental platform has enabled the testing of AI-based NTM prediction algorithms and disruption mitigation systems combining active real-time β_N monitoring with massive gas injection and shattered pellet injection technologies. To suppress NTMs, an NTM recognition algorithm was developed associating with a localized ECRH. A closed looped NTM mitigation was realized with typical parameters I_p~500kA, B_t=1.2 T and $\beta_{N,max}$~2.9. The success rate of online disruption mitigation was further improved by combining AI-based predictors[8] with a massive gas injection (MGI) actuator. The real-time mitigation accuracy of disruptions reached 95.5%, and the experimental results showed that 21 out of 22 consecutive high β_N (>2.8) discharges with disruptions were effectively mitigated.

3.3 Small/no ELM regimes

One of the key challenges of burning plasma operation is to maintain a high core confinement keeping the boundary solution compatible. Towards this purpose, recent work on HL-3 has aimed at establishing other regimes where H-mode confinement can be maintained without large ELMs. These include small-ELM or naturally ELM-free regimes such as enhanced D_α (EDA) H-mode, quiescent H-mode (QH-mode).

3.3.1 H-mode plasmas with small ELMs

A wide variety of small ELMs operation were accessed by tuning plasma upper-triangularity δ_u, edge safe factor q_{95} and plasma density n_e. Statistical analysis in Fig. 4 reveals that small ELMs ($\Delta W_{ELM}>/W_E < 2\%$) preferentially occur at high δ_u, high q_{95}, and high density regime. High q_{95} favours small ELMs, and the small ELMs could be obtained in medium q_{95} as well if the density and triangularity are large enough, but it is not enough to reduce the ELM amplitude by raising only the q_{95} in low triangularity, as displayed in Fig. 4(c). Regime access was shown to transition smoothly from mixed ELMs regime (large ELM mixed with small ELMs during inter-large ELMs phase) to pure small ELMs by increasing plasma density, which is considered to be triggered by the resistive ballooning mode near the separatrix. Another approach to increase the q_{95} to access the grassy ELMs regime. Simulation results indicate that high triangularity is generally associated with an increased peeling-ballooning mode (PBM) threshold, while high q_{95} tends to promote stronger edge shear. This enhanced flow or magnetic shear further contributes to the stabilization of PBMs, thereby suppressing large ELM bursts. Additionally, high density operation leads to elevated resistivity near the separatrix, which can destabilize local instabilities—such as resistive ballooning modes—near the pedestal foot.

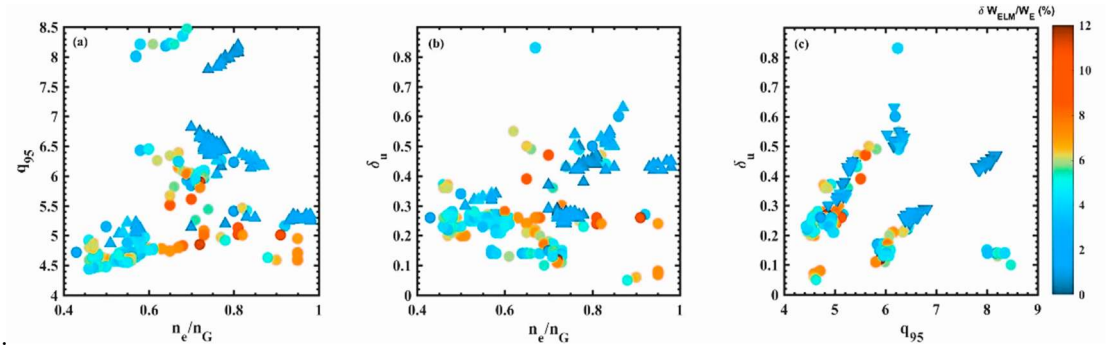

FIG. 4. The dependence of the stored energy loss rate induced by ELMs on upper-triangularity, q_{95} and density normalized by Greenwald limit.

3.3.1 EDA H-mode

EDA H-mode has been achieved in the recent HL-3 experimental campaign, characterized by steady confinement ($H_{98} \approx 1$) without ELMs, and a quasi-coherent mode (QCM) in edge fluctuations. The frequency of QCM evolved from around 60 kHz before transition down to around 20 kHz during ELM free phase transition. This ELM-free H-mode, characterized by an enhanced D_α level, exhibits high energy confinement and is accompanied by a QCM in the edge region, consistent with the typical characteristics of the EDA H-mode.

3.3.2 Quiescent H-mode (QH-mode)

A transient QH-mode was observed with edge harmonic oscillations (EHOs) featuring multiple harmonics (n = 1–4) for the first time on HL-3, with detected dominant frequencies of f_1 = 11 kHz, f_2 = 22 kHz, f_3 = 33 kHz, f_4 = 44 kHz, f_5 = 55 kHz. The ELM-free phase emerged as EHO developed and was sustained even after its disappearance, which were highly correlated with the edge radial electric field profiles. The predictive simulations of QH-mode on HL-3 suggest that the saturated peeling instability could produce an ergodized edge magnetic field region and some convective cells to enhance radial transport and maintain a balanced ELM free edge pedestal[9].

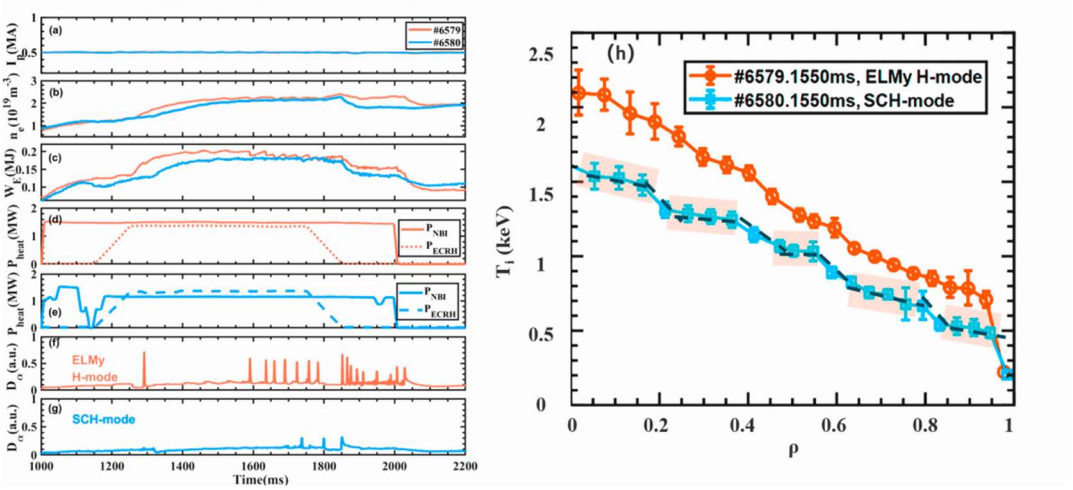

FIG. 5. Time evolutions of the basic plasma parameters: (a) plasma current, (b) line-averaged density, (c) stored energy, (d)-(e) auxiliary heating power, (f)-(g) divertor D_α internsity. (h) The ion temperature profiles in the quasi-steady state measured by the charge exchange recombination spectrum (CXRS) diagnostic system. The upper triangularity is δ_u = 0.35, and total heating power is P_{heat} = 2.9 MW for shot #6579, and δ_u = 0.55, P_{heat} = 2.6 MW for shot #6580, respectively.

3.3.3 'Staircase' H-mode

A novel ELM-free regime which emerged with the T_i profile exhibiting a quasi-periodic step-like structure is termed as 'staircase' H-mode or 'SCH-mode'. This was realized on HL-3 by raising upper triangularity δ_u from 0.35 to 0.55 with low density ($\bar{n}_e \sim 1-2\times10^{19}m^{-3}$). The step-like structure and standard structure of ion temperature profiles across the minor radius are shown by the dashed line and yellow shadow in Fig. 5(h). MHD analysis and modelling indicates that the formation process is closely related with the ubiquitous self-organization mechanism of complex dynamical systems, which are still being analyzed. It was supposed that the SCH-mode effectively decentralizes the enormous risk associated with a single sharp edge layer into a series of meso-scale layers, thus effectively dispersing large edge heat flux and preventing steep edge pedestal structure to maintain an ELM-free state.

4. EFFORT FOR POWER EXHAUST SOLUTION

Effective power exhaust is critical for sustaining high-performance plasmas. HL-3 has implemented advanced divertor geometries and active actuators to mitigate heat loads and control edge-localized modes (ELMs), validating power exhaust solutions compatible with high-performance operation.

4.1 Advanced divertor configurations

Advanced divertor configurations, like snowflake, offer promising solutions by effectively spreading particle flux over a larger surface area, thereby reducing the heat flux on divertor target plates. To reduce target heat flux while maintaining access to high confinement, HL-3 developed and tested several advanced divertor geometries, including snowflake-plus, snowflake-minus, and Tripod configurations. These magnetic geometries enhance flux expansion near the divertor targets and promote volumetric dissipation.

In recent campaigns, HL-3 achieved stable H-mode operation in a tripod configuration with up to 4 MW auxiliary heating. EFIT reconstructions and CCD imaging confirmed the presence of two distinct X-points, with the secondary X-point located above the divertor target, which is a feature unique to the Tripod geometry as shown in Fig. 6. Infrared diagnostics show that when the secondary X-point sits above the target surface, heat flux concentrates near the primary strike point. In contrast, configurations with the secondary X-point below the target lead to a more uniform heat flux distribution, highlighting the sensitivity of exhaust behavior to magnetic topology. Comparative experiments between standard and tripod divertors under equivalent heating power (4 MW) in Fig. 6(c) demonstrate that the tripod configuration can achieve lower peak heat flux due to enhanced magnetic flux expansion, which confirms the divertor's capacity for heat load mitigation and supports its further development for high-power plasma operation. Furthermore, a novel X-point slot closure upper divertor has been designed and will be installed by the next experimental campaign[10]., which is expected to enhance the capacity of power and particle exhaust

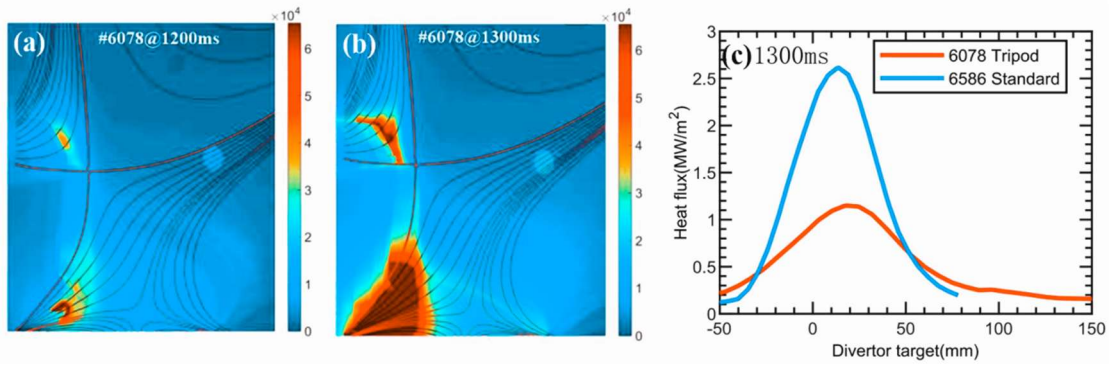

FIG. 6. Infrared camera images and magnetic configuration comparison of a Tripod divertor discharge in HL-3 with (a) heating power below 4 MW; (b) heating power exceeding 4 MW; (c) Comparison of heat flux between the HL-3 standard and the tripod divertor under similar heating power and discharge parameters.

4.2 External actuators for ELM control

Resonant magnetic perturbation (RMP) has been selected as a candidate actuator for ELM control on ITER[11]. Meanwhile, on HL-3, RMPs with toroidal mode numbers $n = 1$ and $n = 2$[12] have been applied during H-mode phase with a 2×4 coil array to mitigate Type-I ELMs, which showed significant impact on L-H transition according to previous observation[13]. The q_{95} widows of ELM control with $n = 1$ and n=2 RMP are different through I_P scanning. The q_{95} window of effective ELM mitigation with $n = 1$ RMP is shown in Fig. 7(a), which is in the range of 4.8 to 7 through stored energy loss ΔW_{ELM} statistics. While for $n = 2$ case, limited data suggests that effective q_{95} window appears near 3.7. Besides, some different features have been observed in $n = 2$ case as shown in Fig. 7 (b), which is, the large ELMs would be mitigated to small (grassy) ELMs with the increasing n_e induced by RMP, which is more significant than the effect of n=1 RMP. A similar simulation work has been performed with 3D perturbed magnetic fields by a biased divertor target system[14]. The simulated case indicates that the ELM control regime can be explained by the combined effects of external perturbations and intrinsic ballooning modes, of which the interactions lead to a redistribution of the mode energy and alter the stability boundary due to their differential effects on plasma profiles. Moreover, the quantitative characterization of how RMPs govern the position and peaking of the divertor heat-flux footprints establishes a robust physical foundation for large heat-load control strategies in future high-performance HL-3 discharges[15].

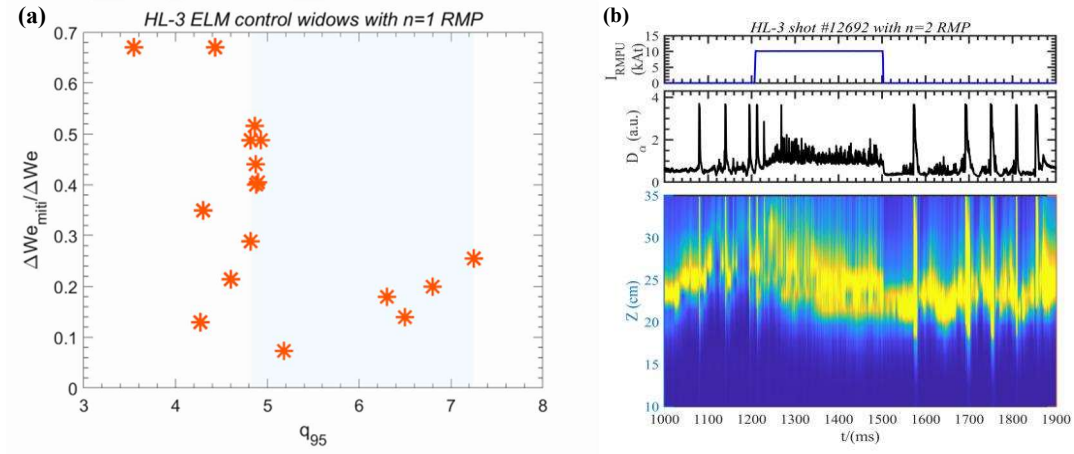

FIG. 7. ELM mitigation with n=1, 2 RMP: (a) the q_{95} range of ELM mitigation with n=1 RMP on HL-3; (b) ELM mitigation by n=2 RMP along with the enhanced D_a radiation.

External impurity seeding via SMBI was performed to control ELMs on HL-3 with neon mixtures. With 30% neon mixed SMBI, each single injected SMB pulse (5 ms pulse width) completely suppressed ELMs for approximately 50 ms without degrading global confinement. Edge diagnostics indicated reduced density fluctuations during the ELM-free phase, with impurities remaining localized near the plasma edge. This is likely attributed to edge dilution and increased shear flow, stabilizing peeling-ballooning modes, which is similar to previous observations on HL-2A tokamak [16].

In addition to RMPs and mixture SMBI, LHW injection on HL-3 has been proved to suppress ELMs while simultaneously improving confinement and reducing divertor heat and particle fluxes[17]. Diagnostic measurements and numerical simulations indicate that LHW heating enhances edge electrostatic turbulence, which increases particle transport in the pedestal region. The resulting pressure profile becomes broader and flatter, stabilizing peeling–ballooning modes that trigger ELMs. ELM suppression scales with turbulence intensity rather than LHW power, confirming this indirect mechanism.

4.3 Divertor detachment

Maintaining divertor detachment during high-power operation is another important approach for component protection. HL-3 has developed a real-time feedback system to monitor and regulate divertor detachment using saturation current (I_{sat}) measurements from divertor Langmuir probes to initiate a preliminary feasibility verification. As illustrated in Fig. 8, the system samples the ion saturation current (I_{sat}) at 100 kHz and processes it through an FPGA-based module. The signal is low-pass filtered at 50 Hz and averaged over 20 ms to yield a 50 Hz control input. The maximum I_{sat} from the probe array is compared to a predefined roll-over threshold I_{roll} to calculate the detaching control criteria $A_{dcc}=I_{sat}^{peak}/I_{roll}$. The resulting error $A_{ref} - A_{dcc}$ against a user-defined target feeds into a proportional–integral (PI) controller, which adjusts the nitrogen injection valve in real time.

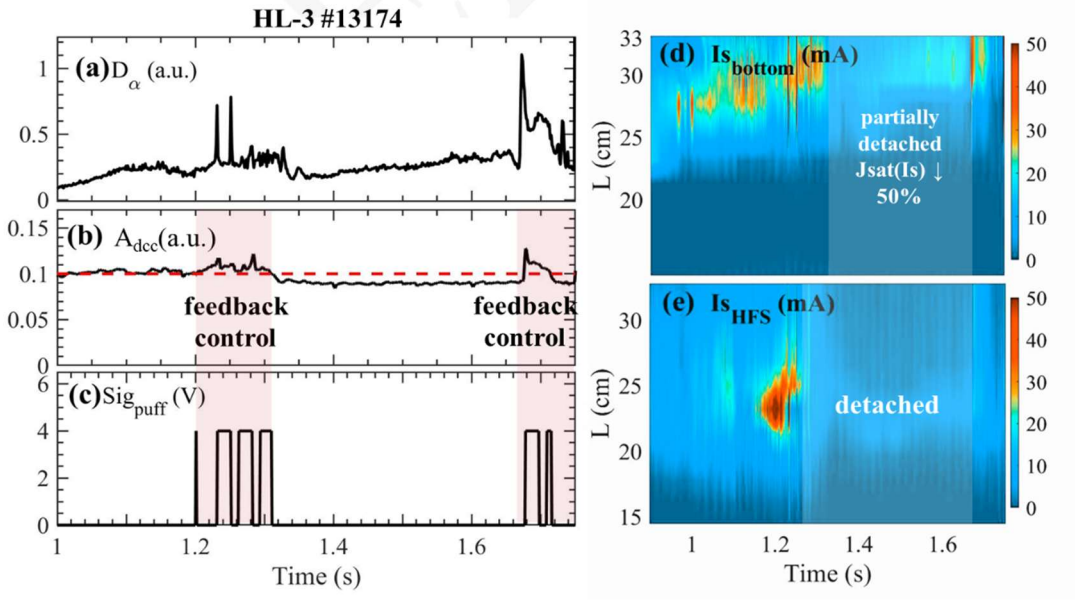

FIG. 8. Time traces of plasma parameters in HL-3 discharge #13174. (a) divertor Dα emission; (b) calculated detaching control criteria A_{dcc} and the threshold($A_{dcc} = 0.1$) to trigger gas puffing; (c)control signal for divertor gas puffing; profiles of ion saturation current (d) on the divertor bottom, and (e) the high-field side.

In this example of divertor parameter feedback control experiment, H-mode was triggered at 1.15 s. When the real-time parameter is detected to be beyond the threshold, the nitrogen gas was seeded. Partial detachment was achieved: saturation current of the divertor bottom of outer target partially detached with a decrease by about 50% (Fig. 8(e)), and fully detachment was observed at the inner target on high field side (Fig. 8(f)), while maintaining stable H-mode. This closed-loop detachment control forms an essential part of integrated exhaust management and supports future operation under more stringent conditions.

5. SUMMARY

Significant progress has been achieved on HL-3 in support of high-performance plasma development and power exhaust solutions for future DT operations. Through a comprehensive upgrade of auxiliary heating, control, and diagnostic systems, the operational capabilities of the device have been greatly expanded. HL-3 has demonstrated high ion temperature operation with core ion temperatures higher than approaching 10 keV in both L-mode (via unfavorable magnetic drift configurations) and H-mode regimes, with triple products reaching 6.7×10^{19} $m^{-3}\cdot s\cdot keV$. The high β_N regime has been realized, e.g., steady operation at β_N ~3 has been demonstrated for longer than 15 energy confinement times that attributed to weak reversed magnetic shear (q_0>1, q_{95}~4.5). Control of instabilities, including NTMs and disruptions, have been enhanced through AI-based real-time systems to maintain high performance of globe confinement.

Scenarios for edge pedestal structure control targeting small/no ELM operation regimes (EDA, QH-mode, staircase ELM free H-mode) have been achieved as well. To ensure compatibility with high-power steady-state operation, HL-3 has developed and validated power exhaust techniques such as advanced divertor geometries, ELM control with RMP, SMBI impurity seeding and LHW, and real-time detachment feedback. These tools are essential for managing heat and particle fluxes in next-step devices.

Looking ahead, HL-3 will further focus on integrated core-edge scenario development under elevated auxiliary power (>40 MW) with enhanced fundamental physical understanding and technical improvements, including achieving high triple product, radiative divertor studies, fast-ion transport investigation, and isotope fuel control. The demonstrated hardware and physics capabilities would establish HL-3 as a key platform for deuterium-tritium burning plasma research.

ACKNOWLEDGEMENTS

The author (W. L. Zhong) would like to acknowledge all those who have contributed to the HL-3 project. Views and opinions expressed are however those of the author(s) only and do not necessarily reflect those of any entities affiliated with the authors.

REFERENCES

[1] Duan X.R. et al Recent advance progress of HL-3 experiments, Nuclear Fusion 64 (2024) 11202
[2] P.L. Liu et al Enhancements in Vertical Instability Control for the HL-3 Tokamak, Journal of Fusion Energy 44 (2025) 2
[3] G.H. Zheng et al Real-time equilibrium reconstruction by multi-task learning neural network based on HL-3 tokamak, Nuclear Fusion 64(2024) 126041
[4] Y. Zhou, et al Quasi-optical design for the cross-polarization scattering diagnostic on the HL-3 tokamak. Review of Scientific Instruments 95 (2024), 53507

[5] Y.R. Zhu et al Nonlinear simulations of the peeling-ballooning instability of super H-modes in the HL-3 tokamak, Nuclear Fusion 64(2024) 096019
[6] Y.P. Zou et al Simulation of β-induced Alfvén eigenmode instabilities and mode transition for HL-3 hybrid scenario, Nuclear Fusion 65 (2025) 026034
[7] S.Q. Wang et al Interaction between MTM and EGAM for energy and particle confinement improvements on HL-3 tokamak, Nuclear Fusion 65(2025) 026013
[8] Z.Y. Yang et al Implementing deep learning-based disruption prediction in a drifting data environment of new tokamak: HL-3, Nuclear Fusion 65 (2025) 026030.
[9] Z. Liang et al Predictive nonlinear MHD simulations of quiescent H-mode plasma in the HL-3 tokamak, Physics of Plasmas 32(2025) 012502
[10] H.L. Du et al Design of an X-point slot closed divertor for the HL-3 tokamak with SOLPS-ITER, Nuclear Fusion 65 (2025) 036023
[11] A. Loarte et al Progress on the application of ELM control schemes to ITER scenarios from the non-active phase to DT operation, Nuclear Fusion 54 (2014) 033007
[12] A. Wang et al Final development and preliminary experiment progress of in-vessel resonant magnetic perturbation coils system on HL-3 tokamak, Fusion Engineering and Design, 208 (2024) 114702
[13] Y. Zhang et al Influence of n = 1 resonant magnetic perturbation on flow and turbulence towards L-H transition, Nuclear Fusion, 65(2025) 066016
[14] J. Huang et al Three-dimensional nonlinear modeling of ELM dynamics with biasing in HL-3 tokamak, Nuclear Fusion 65 (2025) 094001
[15] G.Q. Dong et al Divertor footprint modeling due to RMP in HL-2A and role of plasma response, Nuclear Fusion 65(2025) 016044
[16] W.L. Zhong. et al Impact of impurity mixture gas seeded by supersonic molecular beam injection on edge-localized modes in the HL-2A tokamak, Nuclear Fusion 59 (2019) 076033
[17] Y. M. Zhang et al Impact of lower hybrid wave injection on edge localized modes in the HL-3 tokamak, Nuclear Fusion 65 (2025) 096019